

Antiholons in one-dimensional t - J models.

C. Lavallo¹, M. Arikawa², S. Capponi³, F.F. Assaad^{1,4} and A. Muramatsu¹

¹ *Institut für Theoretische Physik III, Universität Stuttgart, Pfaffenwaldring 58, D-70550 Stuttgart, Germany.*

² *Department of Mathematics and Statistics, University of Melbourne, Victoria 3010, Australia.*

³ *Université Paul Sabatier, Laboratoire de Physique Quantique, 118 route de Narbonne, 31062 Toulouse, France*

⁴ *Max-Planck-Institut für Festkörperforschung, Heisenbergstr. 1, D-70569 Stuttgart, Germany.*

Using a newly developed hybrid Monte Carlo algorithm for the nearest-neighbor (n.n.) t - J model, we show that antiholons identified in the supersymmetric inverse squared (IS) t - J model are clearly visible in the electron addition spectrum of the n.n. t - J model at $J = 2t$ and also for $J = 0.5t$, a value of experimental relevance.

PACS numbers: 71.10.Fd, 71.10.Pm, 71.10.-w

It is well established that electrons in one-dimensional (1D) metals generally lead to a Luttinger liquid [1, 2], where charge-spin separation (CSS) takes place. The most direct evidence of CSS was predicted for the spectral function of such systems [3, 4]. While experimental evidence of CSS has accumulated in recent years [5, 6, 7], an exact theoretical evaluation of the one-particle spectral function $A(k, \omega)$ could until now only be fully accomplished for the Hubbard model at $U = \infty$ for arbitrary doping on the basis of the Bethe-Ansatz solution [8, 9]. However, recent progress was made for spectral properties of the supersymmetric (SuSy) t - J model with $1/r^2$ interaction, where beyond the exact ground state (GS) [10], the thermodynamics [11], the compact support of $A(k, \omega)$ [12], the single-hole dynamics [13], and the electron addition spectrum [14] could be calculated analytically. In addition to spinons and holons, the IS SuSy t - J model was shown to contain antiholons with charge $Q = 2e$, spin $S = 0$, and twice the mass of the holons, i.e. they are not merely charge conjugate to the holons.

We present in this Letter one-particle spectral functions for the 1D n.n. t - J model with finite doping, obtained by quantum Monte Carlo (QMC) simulations based on a newly developed hybrid algorithm. We show that the electron addition part of $A(k, \omega)$ presents a clear structure following the antiholon dispersion found in $A(k, \omega)$ of the IS SuSy t - J model for the same doping. Our results show moreover, that also away from that point, a corresponding feature is present, strongly indicating that antiholons originally identified in the IS SuSy t - J model are generically present in the n.n. model.

The t - J model reads:

$$H_{t-J} = - \sum_{i < j, \sigma} t_{ij} (\tilde{c}_{i,\sigma}^\dagger \tilde{c}_{j,\sigma} + \text{h.c.}) + \sum_{i < j} J_{ij} \left(\vec{S}_i \cdot \vec{S}_j - \frac{1}{4} \tilde{n}_i \tilde{n}_j \right). \quad (1)$$

Here, $\tilde{c}_{i,\sigma}^\dagger$ are projected fermion operators $\tilde{c}_{i,\sigma}^\dagger = (1 - n_{i,-\sigma}) c_{i,\sigma}^\dagger$, $\vec{S}_i = (1/2) \sum_{\alpha, \beta} c_{i,\alpha}^\dagger \vec{\sigma}_{\alpha, \beta} c_{i,\beta}$, $\tilde{n}_i = \sum_{\alpha} \tilde{c}_{i,\alpha}^\dagger \tilde{c}_{i,\alpha}$ and $c_{i,\alpha}^\dagger$ and $c_{i,\alpha}$ are canonical creation and annihilation fermionic operators respectively with $n_{i,\sigma} = c_{i,\sigma}^\dagger c_{i,\sigma}$. We

consider two type of interactions: (i) n.n. type: $t_{ij} = t \delta_{j,i+1}$, $J_{ij} = J \delta_{j,i+1}$ and (ii) IS SuSy type: $t_{ij} = J_{ij}/2 = t(\pi/L)^2 / \sin^2(\pi(i-j)/L)$. L is the length of the system and the lattice constant is unity. For the n.n. model, it is convenient for the development of the algorithm to perform first a canonical transformation [15, 16]

$$c_{i\uparrow}^\dagger = \gamma_i^+ f_i - \gamma_i^- f_i^\dagger, \quad c_{i\downarrow}^\dagger = \sigma_i^- (f_i + f_i^\dagger), \quad (2)$$

where f_i^\dagger, f_i are canonical operators for spinless fermions, $\sigma^\pm = 1/2(\sigma^x \pm i\sigma^y)$, and $\gamma^\pm = 1/2(1 \pm \sigma^z)$, with σ^α , $\alpha = x, y, z$ Pauli matrices. The Hamiltonian (1) becomes:

$$\mathcal{H} = +t \sum_{\langle i,j \rangle} P_{ij} f_i^\dagger f_j + \frac{J}{2} \sum_{\langle i,j \rangle} \Delta_{ij} (P_{ij} - 1), \quad (3)$$

where $\langle i, j \rangle$ means n.n. $P_{ij} = 1/2(1 + \vec{\sigma}_i \cdot \vec{\sigma}_j)$ and $\Delta_{ij} = 1 - f_i^\dagger f_i - f_j^\dagger f_j$. The constraint against double occupancy becomes $\sum_i (1 - \sigma_i^z) f_i^\dagger f_i = 0$, and commutes with the Hamiltonian. We consider now the following definition of an expectation value:

$$\langle \hat{O} \rangle = \lim_{\Theta \rightarrow \infty} \frac{\sum_n \langle \Psi_n | \mathcal{P} e^{-\frac{\Theta}{2} \mathcal{H}} \hat{O} e^{-\frac{\Theta}{2} \mathcal{H}} \mathcal{P} | \Psi_n \rangle}{\sum_n \langle \Psi_n | \mathcal{P} e^{-\Theta \mathcal{H}} \mathcal{P} | \Psi_n \rangle}, \quad (4)$$

where $|\Psi_n\rangle = |s_n\rangle \otimes |\Psi_T\rangle$, with $\{|s_n\rangle\}$ a complete set of spin states and $|\Psi_T\rangle$ a trial wavefunction for the spinless fermions. \mathcal{P} is a projector ensuring the constraint against double occupancy. Taking the limit $\Theta \rightarrow \infty$ leads each state $\mathcal{P} |\Psi_T\rangle \otimes |s_n\rangle$ to converge to the GS as long as the GS has a finite overlap with it. The multiplicity is corrected by the normalization factor. Introducing after slicing in imaginary time (typically time slices $\Delta\tau = 0.1/t$ are used) a complete set of spin states, and checkerboarding, the spin states are represented by world-lines, and for each configuration of them, fermions are evolved exactly since the Hamiltonian (3) is bilinear in fermions. It can be easily shown that the total weight for a given configuration of the world-lines is given by $W_H D_f$, where W_H is the weight of an antiferromagnetic Heisenberg model (AFHM), whereas D_f is a fermionic determinant [17, 18]. The updating of spin world-lines is performed using the

loop-algorithm [19], with the same complexity as for an AFHM, in contrast to a recently proposed pure loop-algorithm [20]. In fact, the autocorrelation time ($\tau \sim 2$ for $L = 30$ and $J/t = 2$) for the internal energy is very similar to the one for the AFHM. Due to the mixed character we denominate the whole hybrid-loop algorithm. Figure 1 shows a comparison of GS energies from QMC and exact diagonalization for various values of J at a density $n = 0.9$. The correct value is reached for values of the projection parameter $\Theta \sim 10/t - 20/t$, demonstrating that the algorithm leads to the correct GS with high accuracy (statistical errors are smaller than the size of the symbols). Dynamical data are obtained from the imaginary time Green's function and analytically continued using the maximum entropy method [21]. Further details will be presented elsewhere [18].

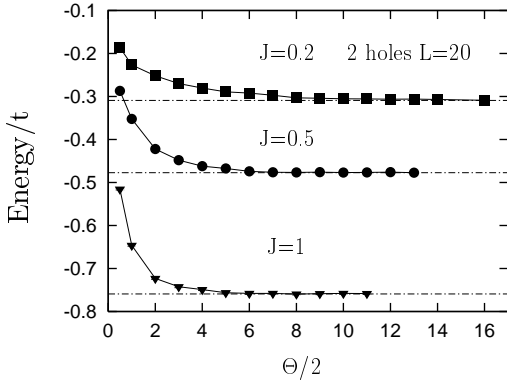


FIG. 1: Ground-state energies *vs.* exact diagonalization results for $L = 20$ with two holes as a function of the projection parameter Θ .

We consider $A(k, \omega)$ both for electron-removal (ER) and electron-addition (EA) processes. Figure 2 a) shows $A(k, \omega)$ obtained from the QMC simulations for $J = 2t$ ($L = 40$, $\Theta = 24/t$), at a density $n = 0.6$. The Fermi energy is taken as the zero of the energy scale. A splitting of the spectral weight into two branches can be readily seen on the EA side, in contradiction with what is expected for a single band. Figure 2 b) shows the projection of $A(k, \omega)$ on the (ω, k) plane, revealing the dispersion of the main features in the spectrum, together with the compact support for the IS SuSy t - J model at the same density. Furthermore, the dispersions of spinon (s), holon (h), and antiholon (\bar{h}) branches that determine the compact support for EA processes in the IS SuSy t - J model are also shown. The dispersions for right (R) and left (L) going spinons and holons are given by $\epsilon_{sR(L)}(q)/t = q(\pm v_s^0 - q)$, and $\epsilon_{hR(L)}(q)/t = q(q \pm v_c^0)$, respectively, where $v_c^0 = \pi(1 - n)$ and $v_s^0 = \pi$. The antiholon dispersion is $\epsilon_{\bar{h}}(q)/t = q(2v_c^0 - q)/2$. The accessible range of momenta is for $\epsilon_{sR(L)}$ and $\epsilon_{hR(L)}$, $0 \leq q \leq k_F$ ($-k_F \leq q \leq 0$), and for $\epsilon_{\bar{h}}$, $0 \leq q \leq 2\pi - 4k_F$ [11, 12, 14]. The compact support is obtained by assuming that the energy and momenta of the particle (EA) or hole (ER) are given by the addition of energy and momenta of s , h , and \bar{h} with the dispersions above [12]. In the ER part

of the spectrum, only the corresponding part of the compact support and the dispersion of an antiholon branch along the support is shown for clarity, since in contrast to the EA processes, where only one spinon, one holon, and one antiholon are present, in the ER part three spinon and holon contributions [12] are possible. Therefore, a large number of features would appear, whose intensity is at the moment unknown, and hence, their importance is difficult to assess. A sharp feature is visible on the ER side that escapes from the compact support of the IS SuSy model. It is due to a holon branch, and as already discussed in the limit of a single hole [22], the actual dispersion of the holon is needed, in order to describe this feature correctly. Also a deviation from the IS SuSy compact support is observed on the EA side at high energies, where the differences in the models is expected to become noticeable. There are however, several features

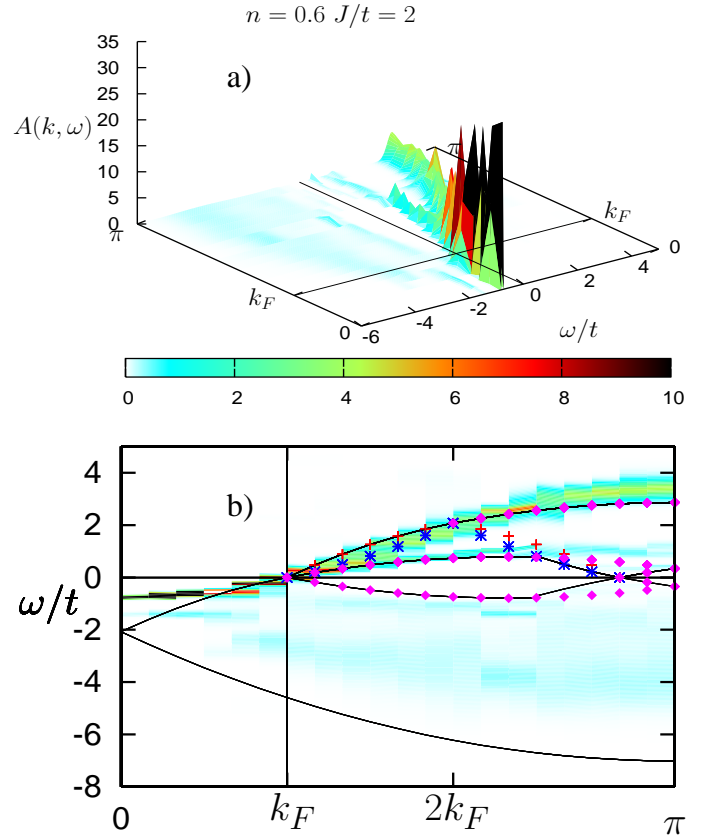


FIG. 2: a) $A(k, \omega)$ for $J = 2t$ at a density $n = 0.6$. b) Projection of intensities on the (ω, k) plane. Solid lines: compact support of the IS SuSy t - J model. Red crosses: spinons, blue asterisks: holons, magenta diamonds: antiholons. See text for the dispersions.

that are well described by the excitations of the IS model. The strongest feature on the EA side is followed closely by the spinon and holon branches between k_F and $2k_F$, and for $k > 2k_F$ by a spinon at k_F together with a dis-

persing antiholon. The analytic results for EA processes in the IS SuSy model [14] show that the largest portion of spectral weight is along this line. More striking is a second, weaker, but clearly visible branch that follows very closely the dispersion of an antiholon between k_F and $2\pi - 3k_F$. The analytic results of $A(k, \omega)$ for the IS SuSy model [14, 23] predict a stepwise discontinuity at this edge and, in fact, the explicit evaluation of the weight shows for the present range of doping a higher value than in the interior of the support. Also the upper edge of the compact support on the ER part, that in the IS model corresponds to an antiholon, is well reproduced, with spectral weight down to very low energies around $3k_F$, as predicted by the IS SuSy model. Therefore, at the SuSy point, the clearest signal of CSS in $A(k, \omega)$ for the n.n. t - J model are present in the EA part of the spectrum and through the comparison with the IS t - J model, it is clear that a sizeable part of the spectral weight goes to the antiholon excitation. Further analytical results

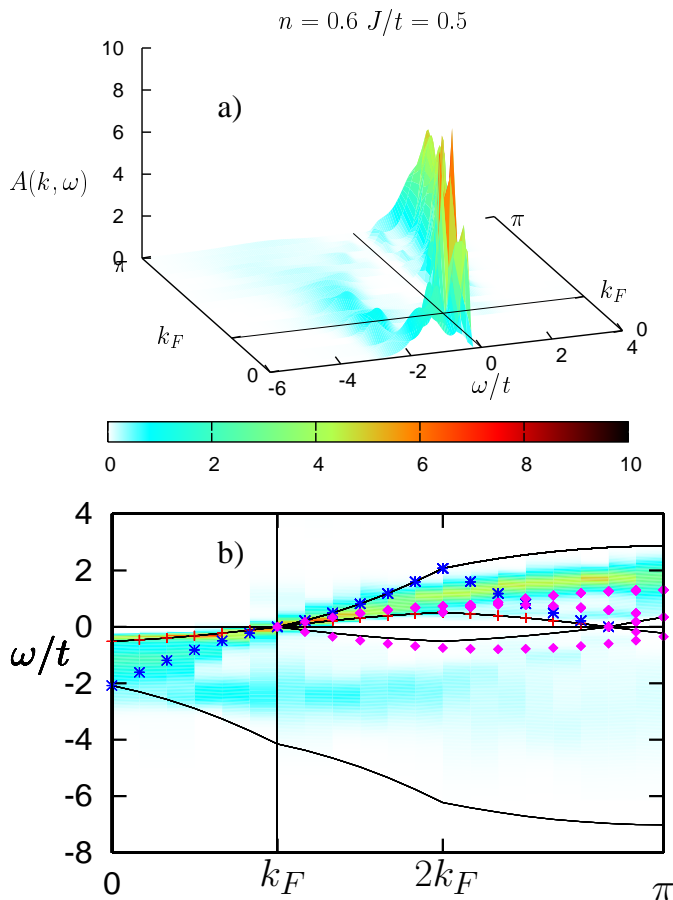


FIG. 3: a) $A(k, \omega)$ for $J = 0.5t$ at $n = 0.6$. b) Projection of intensities on the (ω, k) plane. Symbols coded as in Fig. 2

concerning the detailed structure of $A(k, \omega)$ on the EA part and for the one-holon and one-spinon contributions on the ER part will be published elsewhere [23].

Since the exact solution of the IS model is restricted to the SuSy point, it is of much interest to see whether the

features discussed above correspond to a generic behavior of the n.n. t - J model or whether it is better described, e.g. by the solution of the n.n. model at $J = 0$ [8]. Figure 3 a) shows $A(k, \omega)$ for $n = 0.6$ and $J = 0.5t$ ($L = 40$, $\Theta = 56/t$), i.e. very far away from the SuSy point and at a value of J/t of experimental relevance for cuprate compounds. A perspective was chosen, so that it is already visible that as in the SuSy case, a structure splits off the main feature for k between $2k_F$ and π . Figure 3 b) shows the projection of $A(k, \omega)$ on the (ω, k) plane. As a model for free spinons, holons, and antiholons, we use the same dispersions as for the IS SuSy model, but with $\epsilon_{sR(L)}(q) = (J/2)q(\pm v_s^0 - q)$, i.e. assuming that away from the SuSy point, only the energy scale of spinons is changed. The corresponding compact support, spinon, holon, and antiholon dispersions are encoded as in Fig. 2. In the present case, the compact support encloses rather well all the spectral weight. Moreover, on the ER part, the strongest feature is very accurately followed by a spinon, whereas a second structure is also closely followed by a holon. A more detailed view of these structures is given below in Fig. 4. They correspond to the generally expected signal in photoemission for CSS, that were also found in previous numerical studies of the Hubbard model [24]. However, as shown in Fig. 4, the present algorithm seems to lead to results accurate enough, so that after application of maximum entropy, CSS is seen below E_F in a wider range in k -space than previously. On the EA side, the feature with largest intensity is followed close to k_F by a holon, a spinon, and an antiholon. However, further away from k_F , the dispersion of the maximum is, up to $k \sim 2k_F$, closer to an antiholon going from k_F to $2\pi - 3k_F$ and beyond $2k_F$ by a curve corresponding to a spinon at k_F and a dispersing antiholon. Moreover, a second maximum develops beyond $2k_F$ that follows the antiholon dispersing from k_F to $2\pi - 3k_F$, in a similar way as for $J = 2t$ but with a smaller gap between both curves. In particular, the results from the simulations show appreciable weight between $3k_F$ and the zone boundary, where only antiholons are present.

A closer look to both features signaling CSS is given in Fig. 4. Figure 4 a) shows $A(k, \omega)$ on the ER side and the location of the excitation energies for one spinon and one holon. Whereas the spinon dispersion follows the QMC data very closely, a deviation is seen for the holon for the farthest points from k_F , as can be expected, since at higher energies, details of the dispersion matter in general. Yet, the agreement is good enough to enable an identification of the excitation content of the spectrum. The details of the splitted maxima for $2k_F \leq k \leq \pi$ on the EA side are shown in Fig. 4 b), where both an antiholon dispersing from k_F to $2\pi - 3k_F$ (closer to $\omega = 0$) and an antiholon dispersing from $2k_F$ to $2\pi - 2k_F$ on top of a spinon at k_F are shown. Whereas the latter follows the larger maximum, the former can be associated with the second maximum. As at the SuSy point, there seems to be almost no weight associated with the left propagating spinon and holon that give rise to the con-

tributions between $2k_F$ and $3k_F$. This is consistent with the analytic results obtained for the IS SuSy model [14]. Results for other values of doping ($0.6 \leq n \leq 0.9$) and J ($0.5 \leq J/t \leq 3$) not presented here, show the same qualitative behavior, in particular the presence of a branch on the EA side below the main dispersing structure, that is closely followed by an antiholon branch under the assumption of free spinons, holons, and antiholons.

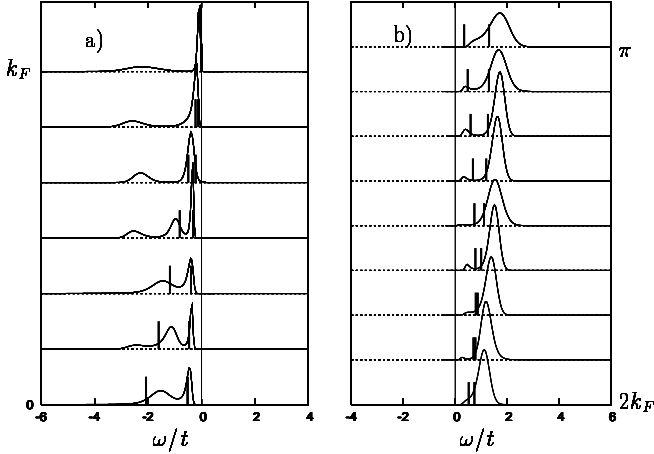


FIG. 4: Detailed view of $A(k, \omega)$ at $J = 0.5t$ and $n = 0.6$. a) ER side for $0 \leq k \leq k_F$ at $J = 0.5t$ and $n = 0.6$. Vertical bars denote the positions for free spinon (closer to $\omega = 0$) and holon excitations. b) EA side for $2k_F \leq k \leq \pi$. Vertical bars denote here antiholon dispersions.

In summary, one-particle spectra for electron-removal and addition were obtained using a new algorithm that delivers accurate dynamical data for the nearest-neighbor t - J model. A comparison with the compact support and excitation content of the $1/r^2$ t - J model at the supersymmetric point $J = 2t$ shows that a new manifestation of charge-spin separation in the n.n. model can be observed in the EA part of the spectrum, where in addition to spinons and holons, a branch following the antiholon dispersion is clearly visible. The same feature is still visible at $J = 0.5t$, where assuming the same dispersions for the holon, and antiholon, as in the IS model but changing the scale of energy to J for the spinon, a fairly good description of the spectrum can be given. Instead, serious deviations result by omitting the antiholon or setting its mass equal to that of the holon (i.e. assuming that it is the charge conjugated counterpart of the holon) [18]. The results above strongly indicate, that antiholons, that are not charge conjugate of holons, are generic excitations in the nearest neighbor t - J model.

We are grateful to M. Brunner for important contributions at early stages of this project. We wish to thank HLR-Stuttgart (Project DynMet) and HLRZ-Jülich for allocation of computer time and SFB 382 for financial support. M.A. acknowledges support by the Visitor Program of the MPI-PKS and Australian Research Council. A.M. is grateful to the ITP, Santa Barbara, for its kind hospitality, and support in part under NSF Grant No PHY99-07949.

-
- [1] F. D. M. Haldane, J. Phys. C **14**, 2585 (1981).
 - [2] J. Voit, Rep. Prog. Phys. **58**, 977 (1995).
 - [3] V. Meden and K. Schönhammer, Phys. Rev. B **46**, 15753 (1992).
 - [4] J. Voit, Phys. Rev. B **47**, 6740 (1993).
 - [5] C. Kim *et al.*, Phys. Rev. Lett **77**, 4054 (1996).
 - [6] K. Kobayashi *et al.*, Phys. Rev. Lett **82**, 803 (1999).
 - [7] R. Claessen *et al.*, Phys. Rev. Lett. **88**, 096402 (2002).
 - [8] K. Penc *et al.*, Phys. Rev. Lett **77**, 1390 (1996).
 - [9] J. Favand *et al.*, Phys. Rev. B **55**, R4859 (1997).
 - [10] Y. Kuramoto and H. Yokoyama, Phys. Rev. Lett. **67**, 1338 (1991).
 - [11] Y. Kuramoto and Y. Kato, J. Phys. Soc. Jpn. **64**, 4518 (1995).
 - [12] Z. N. C. Ha and F. D. M. Haldane, Phys. Rev. Lett **73**, 2887 (1994).
 - [13] Y. Kato, Phys. Rev. Lett **81**, 5402 (1998).
 - [14] M. Arikawa, Y. Saiga, and Y. Kuramoto, Phys. Rev. Lett **86**, 3096 (2001).
 - [15] G. Khaliullin, JETP Lett. **52**, 389 (1990).
 - [16] A. Angelucci, Phys. Rev. B **51**, 11580 (1995).
 - [17] For a review on determinantal algorithms see e.g. A. Muramatsu, in *Quantum Monte Carlo Methods in Physics and Chemistry*, edited by M. P. Nightingale and C. J. Umrigar (Kluwer Academic Press, Dordrecht, 1999).
 - [18] C. Lavallo *et al.*, (unpublished).
 - [19] H. G. Evertz, M. Marcu, and G. Lana, Phys. Rev. Lett **70**, 875 (1993); H. G. Evertz, in *Numerical Methods for Lattice Quantum Many-Body Problems*, edited by D. Scalapino (Frontiers in Physics, cond-mat/9707221, 2002).
 - [20] B. Ammon *et al.*, Phys. Rev. B **58**, 4304 (1998).
 - [21] M. Jarrell and J. Gubernatis, Phys. Rep. **269**, 133 (1996).
 - [22] M. Brunner, F. F. Assaad, and A. Muramatsu, Eur. Phys. J. B **16**, 209 (2000).
 - [23] M. Arikawa (unpublished)
 - [24] M. Zacher *et al.*, Phys. Rev. B **57**, 6370 (1998).